

# **Lattice and grain-boundary diffusions of impurity atoms in BaSi<sub>2</sub> epitaxial layers grown by molecular beam epitaxy**

K. Nakamura<sup>a</sup>, K. Toh<sup>a</sup>, M. Baba<sup>a</sup>, M. Ajmal Khan<sup>a</sup>, W. Du<sup>a</sup>, K. Toko<sup>a</sup>, and T. Suemasu<sup>a,b</sup>

*<sup>a</sup>Institute of Applied Physics, University of Tsukuba, Tsukuba, Ibaraki 305-8573, Japan*

*<sup>b</sup>Japan Science and Technology Agency, CREST, Tokyo 102-0075, Japan*

**Corresponding author:** T. Suemasu

Institute of Applied Physics, University of Tsukuba, Tsukuba, Ibaraki 305-8573, Japan

TEL/FAX: +81-29-853-5111, Email: [suemasu@bk.tsukuba.ac.jp](mailto:suemasu@bk.tsukuba.ac.jp)

## **Abstract**

Al or B layers of a few hundreds of nm in thickness deposited on BaSi<sub>2</sub> epitaxial films on Si(111) substrates were annealed at different temperatures, and the diffusion coefficients of Al and B were evaluated using secondary ion mass spectrometry with O<sup>2+</sup>. We also investigated the effect of post annealing (850 °C, 10 min) of BaSi<sub>2</sub> films on the diffusion coefficients. It was found that both the lattice diffusion and the grain boundary diffusion were decreased by the post-annealing. The plan-view transmission electron microscopy images revealed that the grain size was increased from approximately 0.2 to 0.6 μm by the annealing, and the X-ray diffraction intensities also increased. The activation energies of lattice and grain boundary diffusions in the post-annealed BaSi<sub>2</sub> are 0.63 eV and 0.58 eV for Al, and 4.6 eV and 4.4 eV for B, respectively.

PACS: 78.40.Fy

**Keywords:** A1. Impurity diffusion; A3. Molecular beam epitaxy; B1. Semiconducting silicides; B3. Solar cell

## 1. Introduction

Photovoltaic cell production has been increasing and its market continues to rapidly expand. Approximately 90% of solar cells are made from Si, because Si is an abundant and well-known material in the semiconductor industry. However, the optical absorption layers of crystalline Si (c-Si) solar cells tend to be much thicker than conventional thin-film solar cells, such as CIGS, because the optical absorption coefficient is much smaller for c-Si. Therefore, new materials for high-efficiency thin-film solar cells are of significant interest. Among such materials, we have focused on semiconducting orthorhombic BaSi<sub>2</sub>, which has particularly favorable characteristics for solar cell applications. BaSi<sub>2</sub> has a bandgap of approximately 1.3 eV and a very large optical absorption coefficient, reaching  $3 \times 10^4 \text{ cm}^{-1}$  at 1.5 eV experimentally [1-3]. *a*-Axis-oriented BaSi<sub>2</sub> can be grown epitaxially on Si(111) and S(001) substrates [4-7]. Recently, we successfully achieved large photoresponsivity and internal quantum efficiency exceeding 70% in *a*-axis-oriented BaSi<sub>2</sub> epitaxial layers grown by molecular beam epitaxy (MBE) [8-11]. These results have spurred interest in this material.

The basic structure of a solar cell is a *p-n* junction. Therefore, control of the conductivity of BaSi<sub>2</sub> by impurity doping is a requirement. The carrier concentration of undoped *n*-BaSi<sub>2</sub> is approximately  $5 \times 10^{15} \text{ cm}^{-3}$  [1]. According to Imai and Watanabe [12], substitution of Si in the BaSi<sub>2</sub> lattice is more favorable than substitution of Ba from an energetic point of view by first-principles calculation. In our previous works, the electron

concentration of Sb-doped BaSi<sub>2</sub> was controlled in the range between 10<sup>16</sup> and 10<sup>20</sup> cm<sup>-3</sup> at room temperature (RT). In contrast, Al- and In-doped BaSi<sub>2</sub> show *p*-type conductivity, but the hole concentration was limited up to 3×10<sup>17</sup> cm<sup>-3</sup> [13]. Very recently, we have achieved the hole concentration exceeding 10<sup>19</sup> cm<sup>-3</sup> in B-doped BaSi<sub>2</sub> [14]. Thus, the remaining step is to grow high-quality *p*-type BaSi<sub>2</sub> layers on undoped *n*-type BaSi<sub>2</sub> layers to form a BaSi<sub>2</sub> *p-n* junction. For this purpose, impurity dopants with smaller diffusion coefficient are favorable to realize a very sharp *p-n* junction. However, there have been no reports on diffusion coefficients of impurity atoms in BaSi<sub>2</sub>.

In this study, we aimed to evaluate the lattice diffusion coefficient of *p*-type dopants Al and B using secondary ion mass spectrometry (SIMS) measurement. Grain boundary (GB) diffusion coefficients were also evaluated because GBs exist in the BaSi<sub>2</sub> epitaxial layers on Si(111) due to three epitaxial variants rotated by 120° around the surface normal [6,15].

## 2. Experimental

A two-step growth method was adopted including reactive deposition epitaxy (RDE; Ba deposition on hot Si) for BaSi<sub>2</sub> template layers, and subsequent MBE (codeposition of Ba and Si on Si) at 600 °C to form BaSi<sub>2</sub> epitaxial films on Si(111). Details of the growth procedure have been previously described [6,15].

First, we investigated the post-annealing duration. It is well known that the crystal

quality and electrical properties of MBE-grown  $\beta$ -FeSi<sub>2</sub> films are improved significantly by annealing at temperatures higher than 800 °C [16,17]. Thus, we performed post-annealing in an ultrahigh-vacuum (UHV) chamber at 850 °C for up to 60 min to determine the proper annealing duration. From the  $\theta$ -2 $\theta$  X-ray diffraction (XRD) patterns, we chose to adopt 850 °C for 10 min. The grain size of BaSi<sub>2</sub> was evaluated by plan-view transmission electron microscopy (TEM).

We next investigated the diffusion coefficients using as-grown and post-annealed (850 °C, 10 min) BaSi<sub>2</sub> epitaxial films on Si(111). Al or B layers of a few hundreds of nm in thickness were deposited on undoped BaSi<sub>2</sub> layers at RT. These samples were cut into several pieces and annealed at different temperatures of 300, 400 and 500 °C for 6, 3 and 1 h, respectively, for Al. On the other hand, the diffusion coefficients of B were evaluated only on the post-annealed BaSi<sub>2</sub>. The diffusion coefficients of B were found to be much smaller than those of Al as described later, and thus the annealing for B diffusion was necessary to perform at much higher temperatures such as 775, 800 and 825 °C for 5, 1 and 0.5 h, respectively. These temperatures were close to the post-annealing temperature of 850 °C. Thus, we omitted the evaluation of diffusion coefficients of B in the as-grown BaSi<sub>2</sub>. We investigated the depth profiles of Al and B in BaSi<sub>2</sub> using SIMS measurement with O<sup>2+</sup>, and evaluated the lattice and GB diffusion coefficients of Al and B atoms.

### 3. Results and discussion

Figure 1 shows the  $\theta$ - $2\theta$  XRD patterns of as-grown and post-annealed BaSi<sub>2</sub> films at 850 °C for 10 and 60 min. The peak intensities of the BaSi<sub>2</sub> annealed at 850 °C for 10 min was the largest. The fact that the XRD peak intensities decreased after the 60 min annealing is probably because some amounts of Ba in the BaSi<sub>2</sub> diffused out due to its large vapor pressure during the long-time annealing. From these results, we chose to adopt the post-annealing duration as 10 min. In order to investigate what happened in the BaSi<sub>2</sub> by the post-annealing, we performed plan-view TEM observations. Figures 2(a) and 2(b) show the plan-view bright-field (BF) TEM images of the as-grown and the post-annealed BaSi<sub>2</sub> films, respectively. The incident electron beam was almost parallel to the BaSi<sub>2</sub>[100] zone axis, but was slightly tilted for the GBs to be seen clearly. Note that approximately 120° sharp GBs are present. Detailed discussions about the GBs were given in our previous report [15]. We can see that the grain size of BaSi<sub>2</sub> extended by the post-annealing from approximately 0.2 to 0.6 μm. On the basis of these results, we can say that the post-annealing improved not only the crystalline quality of BaSi<sub>2</sub>, but also increased the grains of BaSi<sub>2</sub>.

We next discussed the diffusion coefficients of Al and B in BaSi<sub>2</sub>. The depth profiles of Al and B are shown in Figs. 3(a)-3(c). Reference samples with a controlled number of Al and B doped in BaSi<sub>2</sub> have not yet been prepared but will be necessary to precisely determine the impurity concentration by SIMS. Although exact Al and B concentrations could not be

obtained, it does not affect the following analysis. From Figs. 3(a) and 3(b), it can safely be stated that the diffusion coefficients of B were much smaller than those of Al, and that the diffusion of Al was suppressed by the post-annealing. In order to fit the experimental SIMS profiles, both lattice and GB diffusions were taken into consideration because we can see clear GBs in the BaSi<sub>2</sub> films in Figs. 2(a) and 2(b). We adopted Eqs. (1) and (2) for fitting the experimentally obtained SIMS profiles. The concentration distribution  $C(x,t)$  of impurity atom due to the lattice diffusion is given by Eq. (1),

$$C(x,t) = C_0 \operatorname{erfc}(x / 2\sqrt{D_l t}) \quad (1),$$

where  $x=0$  is set at the Al(B)/BaSi<sub>2</sub> interface, and  $C_0$  the Al(B) concentration at  $x=0$ ,  $D_l$  the lattice diffusion coefficient, and  $t$  the annealing duration. On the other hand, the concentration distribution due to GB diffusion follows Eq. (2) [18],

$$s\delta D_{GB} = 1.332(D_l / t)^{1/2} \left( -\partial \ln C(x,t) / \partial x^{6/5} \right)^{-5/3} \quad (2),$$

where  $s$  is the segregation factor,  $\delta$  the grain boundary width, and  $D_{GB}$  the GB diffusion coefficient. Figure 4 is an example of the measured and simulated SIMS profiles of Al in the post-annealed BaSi<sub>2</sub> film. Annealing for Al diffusion was performed at 300 °C for 6 h in Fig. 4.

The experimentally obtained depth profile of Al was reproduced relatively well with Eqs. (1) and (2). Note that there are three regions in Fig. 4; the Al layer region, the lattice diffusion region (broken line), and the GB diffusion region (dotted line). Similar fittings were performed for the other samples to evaluate the diffusion coefficients.

The Arrhenius plots for the obtained lattice diffusion coefficient  $D_{\text{Lattice}}$  and the product of segregation factor, GB width and GB diffusion coefficient  $s\delta D_{\text{GB}}$  of Al and B atoms are shown in Figs. 5(a) and 5(b), respectively. In the case of Al diffusion performed on the as-grown BaSi<sub>2</sub> at temperatures higher than 400 °C, it was difficult to fit the experimental profile using the GB diffusion because the two regions of the lattice and GB diffusions were merged. It was found from Figs. 5(a) and 5(b) that the lattice and GB diffusion coefficients of B are much smaller than those of Al, and that the post-annealing suppressed the diffusion of Al. The gradient of the Arrhenius plots in Figs. 5(a) and 5(b) revealed that the activation energies of lattice diffusion of Al and B in the post-annealed BaSi<sub>2</sub> are 0.63 eV and 4.6 eV, respectively, while those of GB diffusion are 0.58 eV and 4.4 eV, respectively. On the basis of these results, we concluded that B is a favorable dopant impurity atom from the view point of its small diffusion coefficients.

#### **4. Summary**

The lattice and GB diffusion coefficients of Al and B atoms were evaluated using the BaSi<sub>2</sub> epitaxial films capped with Al (B) layers. The post-annealing at 850 °C for 10 min increased the grains of BaSi<sub>2</sub> from approximately 0.2 to 0.6 μm. The SIMS depth profiles of Al and B atoms were reproduced relatively well by taking both the lattice and GB diffusions into consideration. The diffusion coefficients of B were much smaller than those of Al,

meaning that B is more favorable than Al as a *p*-type dopant. The activation energies of lattice diffusion of Al and B in the post-annealed BaSi<sub>2</sub> are 0.63 eV and 4.6 eV, respectively, while those of GB diffusion are 0.58 eV and 4.4 eV, respectively.

### **Acknowledgements**

The authors thank Mr. Saito and Ms. Yoshizawa of the National Institute of Advanced Industrial Science and Technology for plan-view TEM observation. This work was supported in part by CREST of JST.

## References

- [1] K. Morita, Y. Inomata, T. Suemasu, *Thin Solid Films* 508 (2006) 363.
- [2] D. B. Migas, V. L. Shaposhnikov, V.E. Borisenko, *Phys. Status Solidi B* 244 (2007) 2611.
- [3] K. Toh, T. Saito, T. Suemasu, *Jpn. J. Appl. Phys.* 50 (2011) 068001.
- [4] R. A. Mckee, F. J. Walker, J. R. Conner, E. D. Specht, D. E. Zelmon, *Appl. Phys. Lett.* 59 (1991) 782.
- [5] R. A. Mckee, F. J. Walker, *Appl. Phys. Lett.* 63 (1993) 2818.
- [6] Y. Inomata, T. Nakamura, T. Suemasu, F. Hasegawa, *Jpn. J. Appl. Phys.* 43 (2004) L478.
- [7] K. Toh, K. O. Hara, N. Usami, N. Saito, N. Yoshizawa, K. Toko, T. Suemasu, *J. Cryst. Growth* 345 (2012) 16.
- [8] W. Du, M. Suzuno, M. A Khan, K. Toh, M. Baba, K. Nakamura, K. Toko, N. Usami, T. Suemasu, *Appl. Phys. Lett.* 100 (2012) 152114.
- [9] Y. Matsumoto, D. Tsukada, R. Sasaki, M. Takeishi, T. Suemasu, *Appl. Phys. Express* 2 (2009) 021101.
- [10] D. Tsukada, Y. Matsumoto, R. Sasaki, M. Takeishi, T. Saito, N. Usami, T. Suemasu, *Appl. Phys. Express* 2 (2009) 051601.
- [11] T. Saito, Y. Matsumoto, M. Suzuno, M. Takeishi, R. Sasaki, N. Usami, T. Suemasu, *Appl. Phys. Express* 3 (2009) 021301.
- [12] Y. Imai, A. Watanabe, *Intermetallics* 15 (2007) 1291.

- [13] M. Kobayashi, Y. Matsumoto, Y. Ichikawa, D. Tsukada, T. Suemasu, *Appl. Physics Express* 1 (2008) 051403.
- [14] M. Ajmal Khan, K O. Hara, K. Nakamura, M. Baba, K. Toh, M. Suzuno, K. Toko, N. Usami, T. Suemasu, *International Conference of Molecular Beam Epitaxy, WeA-1-2*, Nara, Japan, Sept.26, 2012.
- [15] M. Baba, K. Toh, K. Toko, N. Saito, N. Yoshizawa, K. Jiptner, T. Sekiguchi, K. O Hara, N. Usami, T. Suemasu, *J. Cryst. Growth* 348 (2012) 75.
- [16] M. Takauji, N. Seki, T. Suemasu, F. Hasegawa, *J. Appl. Phys.* 96 (2004) 2561.
- [17] M. Suzuno, Y. Ugajin, S. Murase, T. Suemasu, M. Uchikoshi, M. Isshiki, *J. Appl. Phys.* 120 (2007) 103706.
- [18] A. D. Le Claire, *Br. J. Appl. Phys.* 14 (1963) 351.

Figure 1  $\theta$ - $2\theta$  XRD patterns of as-grown, and annealed BaSi<sub>2</sub> films at 850 °C for 10 or 60 min.

Figure 2 Plan-view BF TEM images of (a) as-grown and (b) post-annealed BaSi<sub>2</sub> films. The incident electron beam was almost parallel to the BaSi<sub>2</sub>[100] zone axis, but was slightly tilted for the GBs to be seen clearly.

Figure 3 SIMS depth profiles of Al for (a) as-grown, (b) post-annealed BaSi<sub>2</sub> films.  
(c) SIMS depth profile of B for annealed BaSi<sub>2</sub> films.

Figure 4 Measured and simulated SIMS profiles of Al in the post-annealed BaSi<sub>2</sub> film.  
Annealing for Al diffusion was performed at 300 °C for 6 h.

Figure 5 Arrhenius plots of (a)  $D_{\text{Lattice}}$  and (b)  $s\delta D_{\text{GB}}$  for as-grown and post-annealed BaSi<sub>2</sub>.

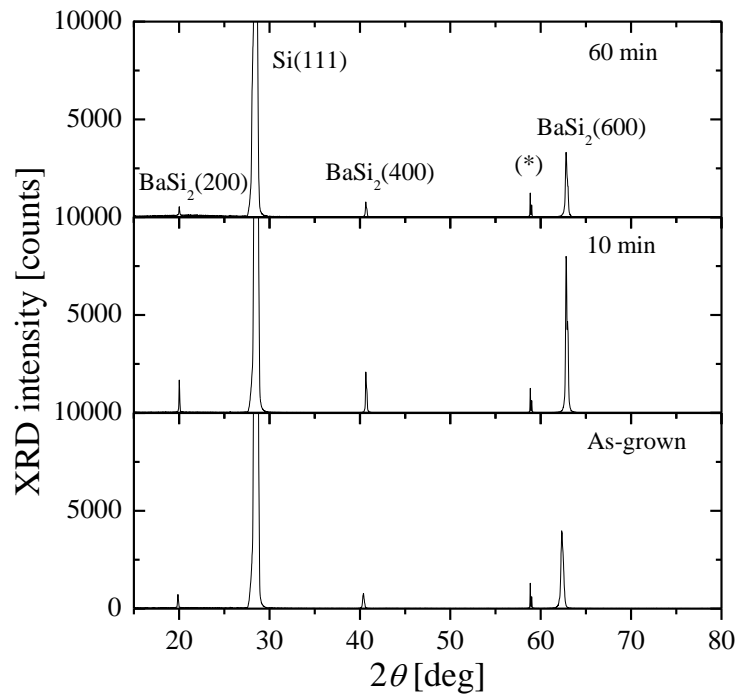
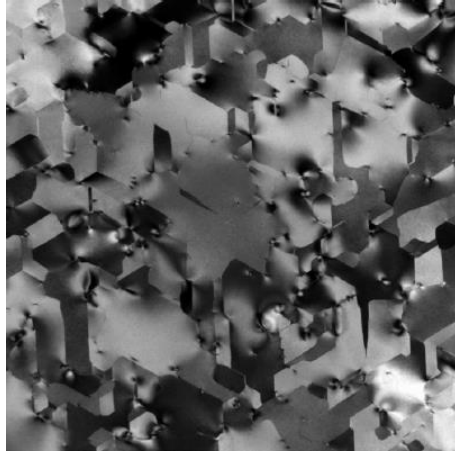
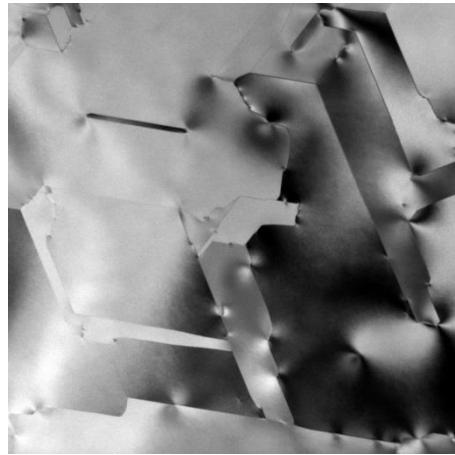


Fig. 1

a



b



200 nm  
—

Fig. 2

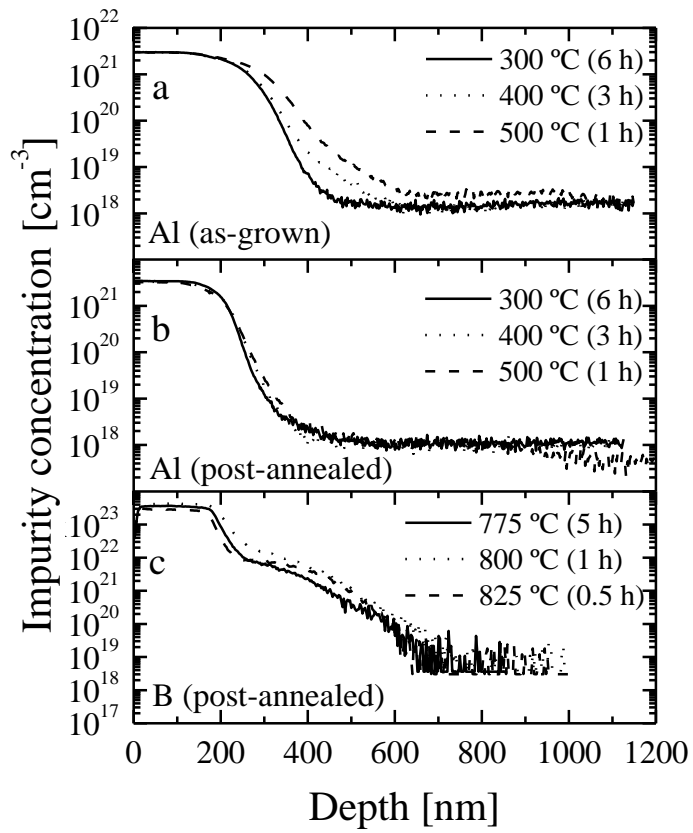


Fig. 3

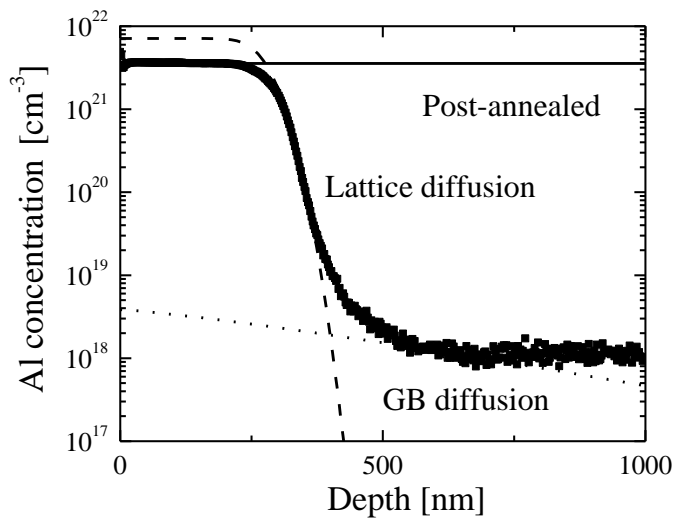


Fig. 4

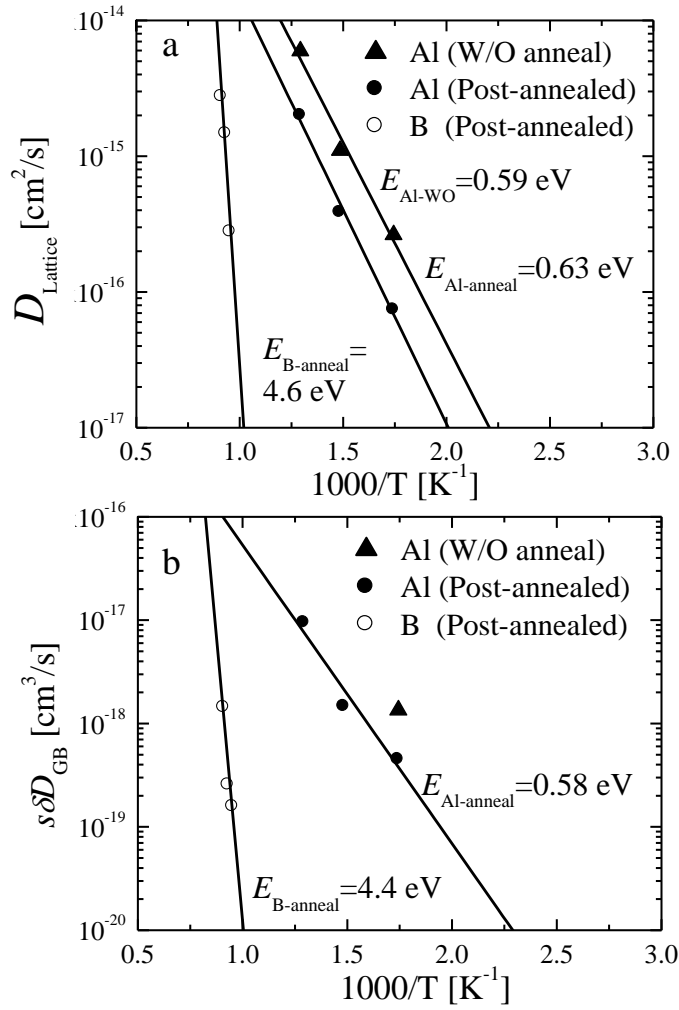


Fig. 5